Structural and denaturation studies of two mutants of a cold adapted superoxide dismutase point to the importance of electrostatic interactions in protein stability

ARTICLE *in* BIOCHIMICA ET BIOPHYSICA ACTA · JANUARY 2014

Impact Factor: 4.66 · DOI: 10.1016/j.bbapap.2014.01.007 · Source: PubMed

8 AUTHORS, INCLUDING:

Antonello Merlino
University of Naples Federico II
129 PUBLICATIONS **1,303** CITATIONS
SEE PROFILE

Irene Russo Krauss
University of Naples Federico II
32 PUBLICATIONS **290** CITATIONS
SEE PROFILE

Immacolata Castellano
Stazione Zoologica Anton Dohrn di Napoli
31 PUBLICATIONS **285** CITATIONS
SEE PROFILE

Filomena Sica
University of Naples Federico II
92 PUBLICATIONS **1,430** CITATIONS
SEE PROFILE

Biochimica et Biophysica Acta 1844 (2014) 632–640

Contents lists available at ScienceDirect

Biochimica et Biophysica Acta

journal homepage: www.elsevier.com/locate/bbapap

Structural and denaturation studies of two mutants of a cold adapted superoxide dismutase point to the importance of electrostatic interactions in protein stability

Antonello Merlino [a,b], Irene Russo Krauss [a], Immacolata Castellano [c], Maria Rosaria Ruocco [d], Alessandra Capasso [d], Emmanuele De Vendittis [d], Bianca Rossi [a], Filomena Sica [a,b,e,*]

[a] Dipartimento di Scienze Chimiche, Università di Napoli "Federico II", Complesso Universitario di Monte Sant'Angelo, I-80126 Napoli, Italy
[b] Istituto di Biostrutture e Bioimmagini, CNR, Via Mezzocannone 16, I-80134 Napoli, Italy
[c] Stazione Zoologica "Anton Dohrn", Villa Comunale, I-80121 Napoli, Italy
[d] Dipartimento di Medicina molecolare e Biotecnologie mediche, Università di Napoli Federico II, Via S. Pansini 5, I-80131 Napoli, Italy
[e] Istituto Nazionale di Biostrutture e Biosistemi, Consorzio Interuniversitario, Viale Medaglie d'Oro 305, I-00136 Roma, Italy

ARTICLE INFO

Article history:
Received 1 August 2013
Received in revised form 7 January 2014
Accepted 10 January 2014
Available online 17 January 2014

Keywords:
Superoxide dismutase
Mutants
Crystal structure
Unfolding
Psychrophilic enzyme
Thermal stability

ABSTRACT

A peculiar feature of the psychrophilic iron superoxide dismutase from *Pseudoalteromonas haloplanktis* (*Ph*SOD) is the presence in its amino acid sequence of a reactive cysteine (Cys57). To define the role of this residue, a structural characterization of the effect of two *Ph*SOD mutations, C57S and C57R, was performed. Thermal and denaturant-induced unfolding of wild type and mutant *Ph*SOD followed by circular dichroism and fluorescence studies revealed that C→R substitution alters the thermal stability and the resistance against denaturants of the enzyme, whereas C57S only alters the stability of the protein against urea. The crystallographic data on the C57R mutation suggest an involvement of the Arg side chain in the formation of salt bridges on protein surface. These findings support the hypothesis that the thermal resistance of *Ph*SOD relies on optimization of charge–charge interactions on its surface. Our study contributes to a deeper understanding of the denaturation mechanism of superoxide dismutases, suggesting the presence of a structural dimeric intermediate between the native state and the unfolded state. This hypothesis is supported by the crystalline and solution data on the reduced form of the enzyme.

1. Introduction

Life at low temperatures requires a vast array of adaptation at molecular and physiological levels. Psychrophilic enzymes are proteins from organisms that inhabit areas with temperatures lower than 20 °C [1–4]. They have to adapt their structure and function to cope with slow reaction rate at low temperatures. The molecular mechanisms of cold adaptation in psychrophilic enzymes are still partially unknown. However, some general features of cold-adapted proteins have been suggested [5–7]. These molecules are endowed with a high conformational flexibility that is often coupled to a reduced thermal stability. The iron superoxide dismutase from *Pseudoalteromonas haloplanktis* (*Ph*SOD) represents an exception to this general rule [8,9]. Although this enzyme comes from an organism living in a hostile habitat (5–15 °C), it presents an unusual thermal stability, which is comparable with that of its mesophilic counterpart from *Escherichia coli* (*Ec*SOD) [8]. Both *Ph*SOD and *Ec*SOD are dimeric metalloenzymes that catalyze the dismutation of superoxide anion radicals into molecular oxygen and hydrogen peroxide [9]. The elucidation of the three-dimensional structure of *Ph*SOD suggested that a major role in its unusually high thermal stability could be played by electrostatic interactions on the protein surface [8]. Recent reviews summarized the structural and functional features of the different families of SODs [10,11].

An interesting feature of *Ph*SOD is the presence in its sequence of a highly reactive cysteine residue (in position 57) that undergoes endogenous glutathionylation upon induction of oxidative stress in *P. haloplanktis* cell cultures [12]. This post-translational modification significantly reduces the inactivation of the enzyme by peroxynitrite, suggesting that this reaction could represent a strategy to improve the antioxidant cellular defense mechanism in the psychrophilic organism. Cys57 belongs to a segment of Fe- and Mn-SODs with a highly variable sequence [9]. To investigate the role of Cys57 in the functional regulation of *Ph*SOD, the mutants C57S and C57R, where the cysteine on the protein surface (Fig. 1) is replaced by serine or arginine, were produced and characterized. Furthermore, the adducts formed by reaction with β-mercaptoethanol [9] and glutathione [12] were analyzed. Substitution of the sulfhydryl group with an oxydryl one did not affect the *Ph*SOD enzymatic activity, whereas the substitution of Cys with Arg causes a slight reduction of the activity [12].

* Corresponding author at: Department of Chemical Sciences, University of Naples "Federico II", Complesso Universitario di Monte Sant'Angelo, I-80126 Napoli, Italy. Tel.: +39 081674479.
E-mail address: filomena.sica@unina.it (F. Sica).

1570-9639/$ – see front matter © 2014 Elsevier B.V. All rights reserved.
http://dx.doi.org/10.1016/j.bbapap.2014.01.007

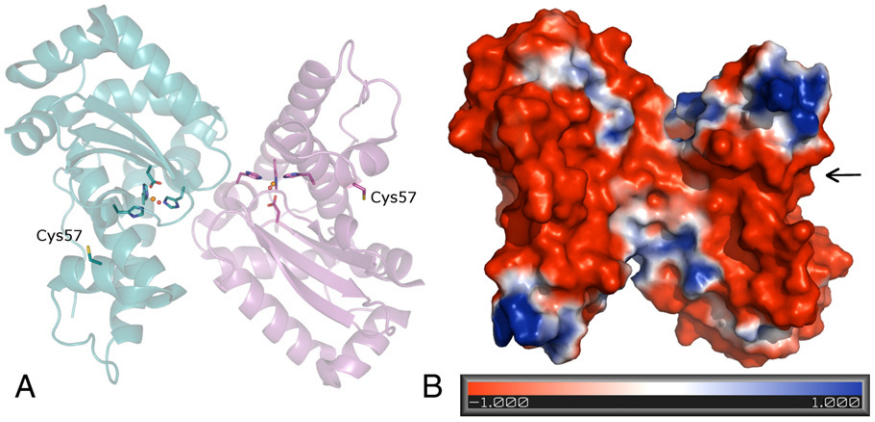

Fig. 1. (A) Overall structure of *Ph*SOD. The two subunits are colored cyan and magenta respectively, active site residues and cysteine 57 are also shown as sticks, iron atoms and the coordinated water molecules are shown as spheres. (B) *Ph*SOD electrostatic surface. Position of Cys57 in one of the two subunits is indicated by an arrow.

Previous results on SODs have suggested a major role for Cys residues in irreversible protein aggregation [13,14]. To complete the characterization of *Ph*SOD, we have now performed a combined structural and biochemical study, in solution and in the crystal state, of the two mutants. Moreover we solved the structure of the reduced form of the enzyme (Fe(II)*Ph*SOD). No significant variation in the structural features of the protein has been found in the Fe(II) form. CD data confirm that *Ph*SOD thermally unfolds through a three-step mechanism and show that the mutation C57R enhances the stability of the native dimer, but destabilizes the intermediate partially unfolded dimer. This finding has been interpreted on the basis of the crystal structure of the mutants.

2. Methods

2.1. Crystallization and data collection

Wild type *Ph*SOD and its mutants containing the replacement of Cys57 with Arg or Ser, hereafter named C57R and C57S, were prepared as previously described [8,9]. Crystals of *Ph*SOD and C57S were obtained by hanging drop vapor diffusion method [15], by using the procedure previously reported [16]. Briefly, crystals were grown in 1.8–2.0 M ammonium sulfate, 1.0–1.2 M NaCl, 100 mM Hepes pH 7.2–7.5. Crystals of C57R were grown by hanging drop vapor diffusion method in the same crystallization conditions (C57R-I) and also in 23% PEG8K, 0.2 M ammonium sulfate, 0.1 M sodium cacodylate pH 7.0 (C57R-II). The reduced form (Fe(II)*Ph*SOD) was obtained by soaking *Ph*SOD crystals in a holding solution containing an excess of dithionite, according to the procedure described in a previous paper [17].

Diffraction data on C57S, C57R-I and Fe(II)*Ph*SOD were collected on a Saturn944 CCD detector at the Istituto di Biostrutture e Bioimmagini (CNR, Naples, Italy) with Cu$K\alpha$ X-ray radiation from a Rigaku Micromax 007 HF generator, whereas those on C57R-II were collected at the Elettra synchrotron, Trieste (Italy). All the crystals were mounted in nylon loops and flash-frozen at 100 K in a nitrogen gas produced by an Oxford Cryosystems Cryostream and maintained at 100 K during the data collection. Crystals were flash-cooled after the addition of 400 mg/ml trehalose to the harvesting solution, with the only exception of crystals of C57R-II that were flash-cooled after the addition of 25% glycerol. Data were processed by HKL2000 [18]. Statistics describing the other crystallographic data are reported in Table 1.

2.2. Structure solution and refinement

Given the strict isomorphism with the wild type protein, the phase determination was carried out by the difference Fourier method. The refined coordinates of *Ph*SOD (PDB IDs: 3LIO and 3LJF, [8]) were used as starting models. The refinement was carried out with CNS [19] and Refmac5 [20] programs. Several alternating cycles of positional refinement, energy minimization, individual temperature factor refinement and manual model building were performed. Model building was done using "O" [21] and "Coot" [22]. Water molecules and trehalose molecules were located in difference Fourier maps and added to models. PROCHECK [23] was used to analyze the quality of the final structures. The refinement statistics are presented in Table 2. The coordinates of C57S, C57R-I, C57R-II and Fe(II)*Ph*SOD were deposited in the Protein Data Bank (PDB IDs: 4L2B, 4L2C, 4L2A, and 4L2D, respectively). C57R-I and Fe(II)*Ph*SOD crystals contain two dimers in the asymmetric unit, whereas the others contain a single dimer in the asymmetric unit.

The figures were drawn using PyMOL (http://pymol.org).

2.3. Guanidine hydrochloride- and urea-induced denaturation studies

Protein concentration has been determined spectrophotometrically from absorbance at 280 nm and using a molar extinction coefficient $\varepsilon = 2.561$ ml/(mg·cm). UV spectra were recorded on a Jasco V-560 spectrophotometer.

Protein samples (0.1 mg/ml in 10 mM Tris/HCl buffer at pH 7.8) were incubated overnight with increasing concentration of guanidine hydrochloride (GdnHCl) (0–5.6 M) or urea (0–7.8 M) at 20 °C.

A non-linear least-square analysis was used to fit the unfolded protein fraction versus the denaturant concentration curves and to

Table 1
X-ray diffraction data-collection and processing statistics.

	C57S (4L2B)	C57R-I (4L2C)	C57R-II (4L2A)	Fe(II)*Ph*SOD (4L2D)
Space group	$P2_1$	$P2_1$	$P2_1$	$P2_1$
Cell parameters				
a (Å)	46.72	50.49	45.62	50.30
b (Å)	103.44	103.77	103.74	103.62
c (Å)	50.53	89.83	50.24	89.34
α (°)	90	90	90	90
β (°)	108.0	103.6	108.3	103.7
γ (°)	90	90	90	90
Resolution range(Å)	30.0–1.97 (2.04–1.97)	50.0–1.66 (1.72–1.66)	50.0–2.06 (2.13–2.06)	30.0–2.07 (2.04–2.07)
Observations	107,691	261,688	96,935	268,327
Unique reflections	30,651	95,529	27,167	53,308
Completeness (%)	95.1 (90.0)	90.1 (76.7)	98.8 (90.4)	98.2 (85.6)
I/σ (I)	9 (3)	8 (3)	13 (4)	9 (4)
Redundancy	3.5 (2.8)	2.7 (2.3)	4.0 (3.2)	5.0 (3.7)
R_{merge} (%)	9.9 (26.9)	9.6 (31.4)	7.4 (23.5)	10.8 (20.5)
Mosaicity	0.8	0.7	0.7	1.2
Molecules in the asymmetric unit	1 dimer	2 dimers	1 dimer	2 dimers

Table 2
Refinement statistics.

	C57S (4L2B)	C57R-I (4L2C)	C57R-II (4L2A)	Fe(II)*Ph*SOD (4L2D)
Resolution range (Å)	20.0–1.97	30–1.66	30–2.06	30–2.07
Number of reflections (F > 0σ(F))	28,084	90,878	25,921	53,243
Number of reflections in test set	2800	4570	2571	2662
R-factor/R-free	0.19/0.24	0.20/0.24	0.19/0.24	0.19/0.24
Number of protein atoms	3022	6151	3031	6039
Water sites	403	911	338	623
Trehalose molecules	2	4	–	4
Rmsd from stereochemical target values				
Bond length (Å)	0.007	0.006	0.022	0.025
Bond angles (°)	1.29	1.89	1.92	2.12
Average B-factor (Å^2)				
Protein, overall	16.73	15.68	22.79	20.05
Main chain	16.23	15.04	22.53	19.23
Side chain	17.25	16.32	23.06	20.90
Solvent atoms	29.41	26.08	34.86	26.25
Ions	12.58	12.07	16.88	15.14
Ligand atoms	33.04	28.46	–	29.37
Ramachandran statistics				
Number of residues in favored region (%)	96.3	97.2	97.1	97.1
Number of residues in allowed region (%)	3.7	2.5	2.9	2.8
Number of residues in outlier region (%)	0	0.3	0	0.1

determine the concentration of the denaturant at the midpoint of denaturation ($C_{1/2}$). The unfolded protein fraction was calculated as follows:

$$F_{un} = \frac{F_{obs} - F_n}{F_u - F_n}$$

where: F_{un} is the unfolded fraction, F_{obs} is the observed value of the signal (CD or fluorescence) at the given denaturant concentration, F_n and F_u are the signal values of the native and completely unfolded state (highest concentration of denaturant), respectively.

2.3.1. Fluorescence measurements

Fluorescence spectra were recorded with a thermostatically controlled JASCO FP-750 spectrofluorometer using a path length of the cell = 1 cm. The emission spectra of C57S and C57R were recorded from 310 to 450 nm and collected at protein concentration 0.035 mg/ml. The measurements have been compared with those already collected on wild-type enzyme [8]. Tryptophan residues were selectively excited at 295 nm, whereas both tyrosine and tryptophan residues were excited at 280 nm.

2.3.2. Circular dichroism

The chemical-induced denaturation curves of C57S and C57R were obtained at constant temperature by recording the CD signal at 222 nm for each independent sample at 0.1 mg/ml protein concentration. CD spectra were recorded on a JASCO J-710 spectropolarimeter equipped with a Peltier thermostatic cell holder (Model PTC-348WI). Before the measurements the instrument was calibrated with an aqueous solution of d-10-(+)-camphorsulfonic acid at 290 nm.

2.4. Thermal denaturation studies

Thermal denaturation of *Ph*SOD, C57R and C57S mutants was monitored by following the change in ellipticity at 222 nm over the temperature range 10–105 °C, with a scan rate of 0.5 °C/min. The reversibility of the transition was then checked by lowering the temperature. Thermal unfolding curves were recorded on 0.1–0.2 mg/ml enzyme solutions in 7 mM Tris/HCl buffer at pH 7.8. Melting temperatures (T_m) were calculated from the second derivative of the ellipticity change vs temperature.

Thermal denaturation of the enzyme samples (0.15 mg/ml in 20 mM Tris/HCl buffer at pH 7.8) was also followed by means of fluorescence measurements realized on a Cary Eclipse fluorescence spectrophotometer (Varian), equipped with an electronic temperature controller. The increase in temperature was set up at 0.2 °C/min, and fluorescence was recorded at every 0.5 °C increase. Excitation wavelength was set up at 280 nm, whereas emission was recorded at 333 nm and 345 nm.

2.5. Thermal inactivation studies

Samples of *Ph*SOD, C57S and C57R at 0.02 mg/ml in 20 mM Tris/HCl buffer at pH 7.8 were incubated for 10 min at various temperatures ranging between 30 and 70 °C and then they were chilled on ice for at least 30 min. The residual activity of the treated samples was assayed at 25 °C by the inhibition of the cytochrome *c* reduction caused by the superoxide anions generated with the xanthine/xanthine oxidase method [24,25]. The activity was expressed as a percentage of that measured on untreated samples.

3. Results

3.1. Solution studies

A previous investigation showed that *Ph*SOD possesses a mixed helix-β-sheet structure [8]. The circular dichroism (CD) spectral features of the two mutants, C57R and C57S, are unchanged with respect to those previously reported for the wild-type enzyme. To verify the effect of mutations on the protein thermal stability, CD spectra were recorded and the signal intensity at 222 nm was followed at increasing temperature from 10 °C to 105 °C. Protein samples underwent irreversible aggregation during thermal unfolding. The spectra recorded at 105 °C revealed the complete loss of secondary structure. The superimposition of denaturation curves of C57S, C57R and *Ph*SOD is shown in Fig. 2. As expected on the basis of the *Ph*SOD behavior [8], the inspection of the melting curves unequivocally indicates that the thermal unfolding of both mutants and wild type enzyme is not a simple two-state process: indeed, all curves present two inflection points (i.e., T_{m1} and T_{m2}), indicative of two temperature-induced transitions. After the first transition, the protein retains a dimeric state, as judged by size exclusion chromatography analysis. Indeed, these enzymes eluted as dimers even after their incubation for 30 min at 65 °C (not shown). The values of the apparent melting temperature (T_{m1} and T_{m2}) for the

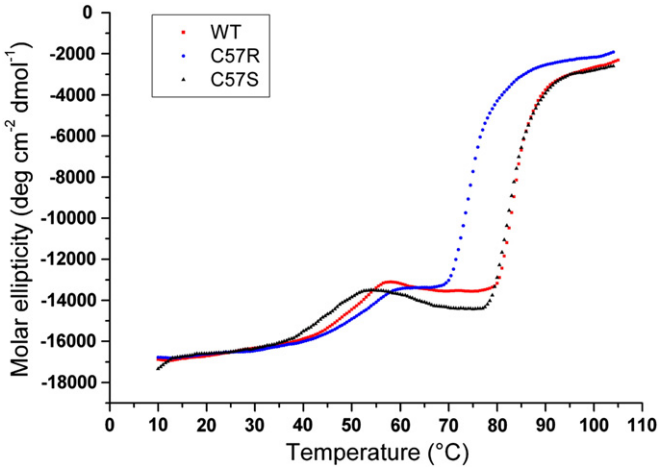

Fig. 2. Thermal unfolding curves of *Ph*SOD, C57R and C57S as followed by CD spectroscopy at 222 nm.

Table 3
Summary of the thermal stability of wild-type *Ph*SOD and its mutants.

	Data obtained by CD measurements			Data obtained by fluorescence measurements
	T_{m1} (°C)	T_{m2} (°C)	$T_{m2} - T_{m1}$ (°C)	T_m (°C)
*Ph*SOD	52 ± 2	83 ± 4	29 ± 4	48 ± 2
C57S	51 ± 2	82 ± 2	31 ± 2	45 ± 2
C57R	55 ± 2	71 ± 3	16 ± 3	52 ± 2

Melting temperatures are averaged on at least three different unfolding temperature profiles.

transitions (see Table 3) indicate a similar thermal stability for C57S and *Ph*SOD [8]. On the other hand, C57R displays a different behavior. In particular, C57R exhibits an increase in T_{m1} from 52 °C to 55 °C with respect to *Ph*SOD, whereas the value of T_{m2} decreases from 83 °C to 71 °C (Table 3).

A focus on the thermal stability was also realized through fluorescence measurements. The thermal treatment of the enzymes provoked a progressive increase of the fluorescence emission and a concomitant red shift of the emission maximum from 333 nm to 345 nm (data not shown). As shown in Fig. 3 the profile of the emission intensity at these wavelengths as a function of temperature is characterized by a single transition. The calculated melting temperatures (Table 3) show that C57R has the highest resistance to heat denaturation, followed by *Ph*SOD and C57S. Thermal unfolding data have been also compared with the heat inactivation profiles of *Ph*SOD and its mutants (Fig. 4). Also in this case, C57R had the highest resistance, followed by C57S and *Ph*SOD; indeed, the calculated half inactivation temperature for C57R was 58 °C, whereas lower values, 55 °C and 54 °C, were calculated for C57S and *Ph*SOD, respectively. Therefore, all these data indicate that heat unfolding and inactivation of *Ph*SOD and its mutants are apparently concomitant processes and point to the highest resistance of C57R to the thermal treatment.

Intrinsic fluorescence emission spectra were used to detect the changes in microenvironments of Tyr and Trp residues as a function of GdnHCl and urea concentration. The fluorescence spectra of both C57R and C57S mutants are characterized by a broad band similar to that of the wild type enzyme [8], indicating that Tyr and Trp residues are in an apolar environment, in agreement with observations based on their X-ray structures. A significant red-shift of the emission maximum

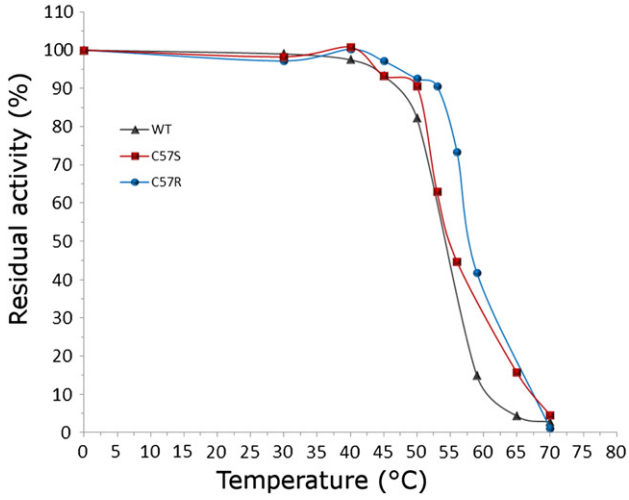

Fig. 4. Heat inactivation profiles of *Ph*SOD, C57R and C57S. The residual SOD activity of the samples was reported as a function of the temperature of heat treatment.

wavelength appears when increasing concentrations of either urea or GdnHCl are added to the protein. This suggests that during protein unfolding significant changes in the microenvironments of fluorophores occur: at high denaturant concentration these residues become fully exposed to the solvent. The unfolding transition curves of *Ph*SOD and its mutants C57S and C57R, obtained by plotting the unfolded fraction against the denaturant concentration, are reported in Fig. 5. Differently from the three-state unfolding reflected by the thermal denaturation CD study, a two-state transition is observed following the change of the fluorescence emission maximum wavelength in the presence of increasing concentration of denaturant. In this case, a full recovery of all the spectroscopic features of the native state is observed upon complete removal of the denaturant by ultracentrifugation. As shown in Fig. 5A, C57R is more resistant to GdnHCl-induced unfolding than C57S and *Ph*SOD. On the contrary, C57S and C57R are less resistant to the action of urea as a chemical denaturant when compared to *Ph*SOD (Fig. 5B). The values of denaturant concentration at the midpoint of the unfolding curve ($C_{1/2}$) for C57R, C57S and *Ph*SOD using either urea or GdnHCl are reported in Table 4. The observed differences in denaturing action of

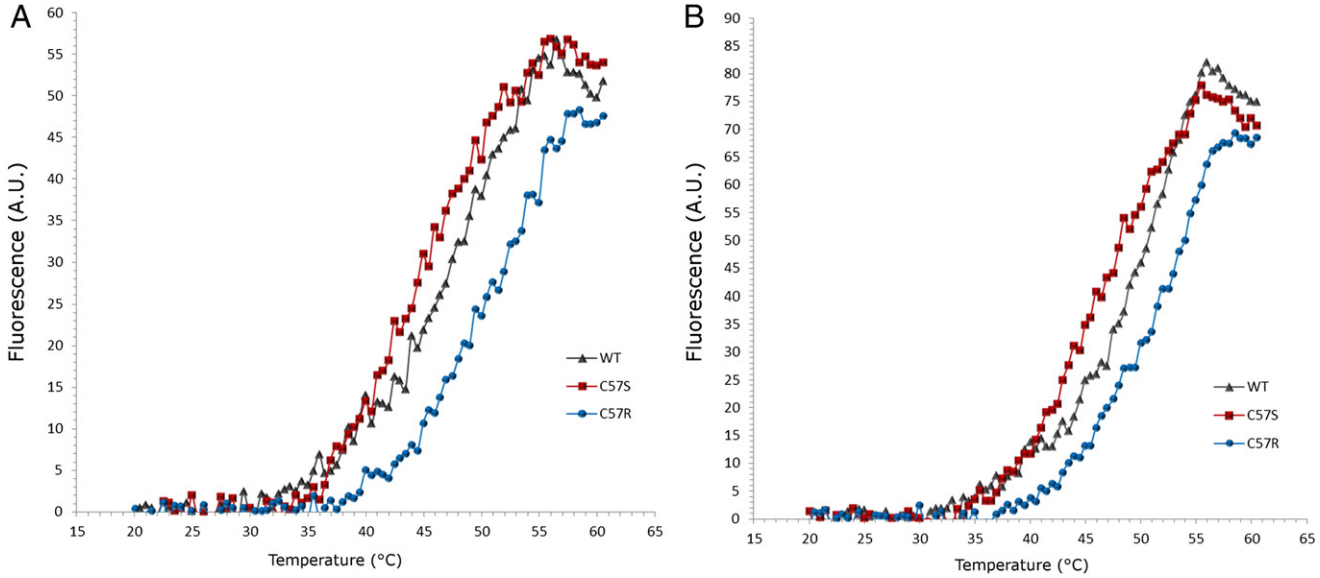

Fig. 3. Fluorescence melting curves of *Ph*SOD, C57R and C57S by monitoring the change of emission at 333 nm (A) and at 345 nm (B). Fluorescence was expressed as arbitrary units and corrected for temperature-dependent quenching of the quantum yield.

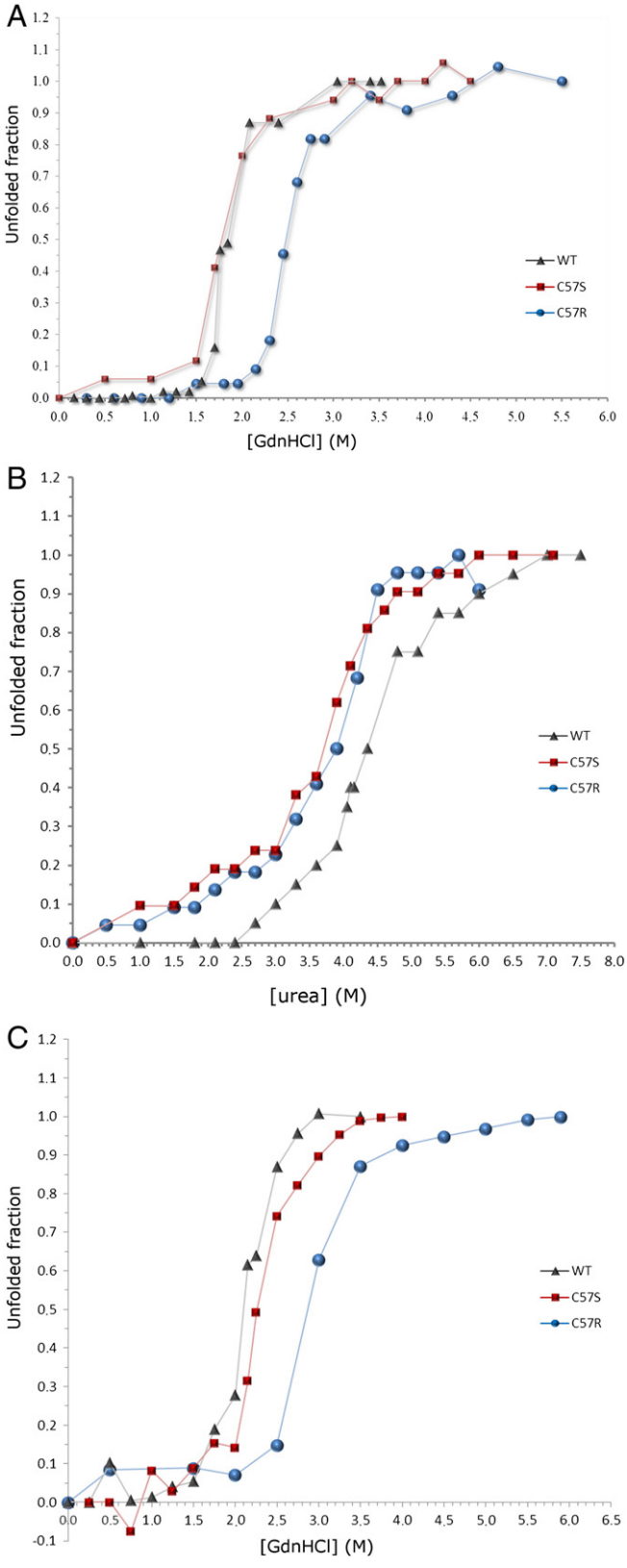

Fig. 5. (A) Unfolding curves of *Ph*SOD, C57R and C57S as followed by monitoring the shift of fluorescence emission maximum wavelength (λ_{exc} = 295 nm) at increasing concentrations of guanidine hydrochloride. (B) Unfolding curves of *Ph*SOD, C57R and C57S as followed by monitoring the shift of fluorescence emission maximum wavelength (λ_{exc} = 295 nm) at increasing concentrations of urea. (C) Unfolding curves of *Ph*SOD, C57R and C57S as followed by monitoring the change of molar ellipticity at 222 nm at increasing concentrations of guanidine hydrochloride.

Table 4
Values of denaturant concentration at half-completion of the transition ($C_{1/2}$) characterizing the chemical-induced denaturation of C57R, C57S and *Ph*SOD.

Protein	Denaturant	Method	$C_{1/2}$ (M)
*Ph*SOD	GdnHCl	Fluorescence (λ_{exc} = 280 nm)	1.79 ± 0.03
		Fluorescence (λ_{exc} = 295 nm)	1.84 ± 0.02
		$CD[\theta]_{222}$	2.13 ± 0.03
	Urea	Fluorescence (λ_{exc} = 280 nm)	4.16 ± 0.05
		Fluorescence (λ_{exc} = 295 nm)	4.22 ± 0.06
C57R	GdnHCl	Fluorescence (λ_{exc} = 280 nm)	2.44 ± 0.03
		Fluorescence (λ_{exc} = 295 nm)	2.49 ± 0.02
		$CD[\theta]_{222}$	2.89 ± 0.04
	Urea	Fluorescence (λ_{exc} = 280 nm)	3.78 ± 0.09
		Fluorescence (λ_{exc} = 295 nm)	3.85 ± 0.07
C57S	GdnHCl	Fluorescence (λ_{exc} = 280 nm)	1.81 ± 0.15
		Fluorescence (λ_{exc} = 295 nm)	1.79 ± 0.04
		$CD[\theta]_{222}$	2.30 ± 0.04
	Urea	Fluorescence (λ_{exc} = 280 nm)	3.73 ± 0.08
		Fluorescence (λ_{exc} = 295 nm)	3.72 ± 0.07

GdnHCl and urea are in line with the different chemical nature of the two denaturants. The secondary structure stability of C57S and C57R was also monitored in the presence of GdnHCl by means of CD spectroscopy, following the change of ellipticity at 222 nm (Fig. 5C). The $C_{1/2}$ values obtained with this method are in agreement with those obtained by fluorescence measurements (see Table 4).

3.2. Structural analysis

The composition of the final refined models of C57R-I, C57R-II, and C57S is summarized in Table 2. The three-dimensional structures of the two mutants are extremely similar, yielding root mean square deviations (rmsd) in CA atom position in the range of 0.27–0.40 Å when the whole dimers are superimposed. The models are essentially isostructural to that of *Ph*SOD (rmsd 0.20 Å, 0.36 and 0.37 Å, comparing *Ph*SOD with C57R-I, C57R-II and C57S, respectively). They adopt the typical Fe/Mn-SODs topology, with the two monomers related by a dyad axis (Fig. 1). The metal-ion coordination sphere is conserved with respect to the wild-type protein, with the side chains of residues His26, His73, Asp157, His171, along with a conserved water molecule, arranged in a trigonal bipyramidal geometry. The only really significant difference between the structure of the mutants and that of *Ph*SOD is confined to the mutation site; therefore, this region accounts for the observed differences in thermal and chemical stability of the proteins. The omit Fo–Fc electron density maps of the mutation sites are reported in Fig. 6. In both subunits of C57S, OH atom of Ser57 is hydrogen bonded to the backbone oxygen of Glu53 (Fig. 6A). In C57R-II, the side chain of Arg57 adopts two different conformations in the two subunits: it forms salt bridges with Asp148 in chain A and with Glu53 in chain B (Fig. 6B and C, respectively). Different results are obtained in the structure C57R-I. In particular, in one out of the two dimers in the asymmetric unit (a.u.) Arg57 interacts with Asp148 in chain A (Fig. 6D) and with Leu145 in chain B (Fig. 6E). In the other dimer, Arg57 adopts two alternative conformations in each subunit. In one case, it is in contact with Glu53; in the other one, it interacts with Asp148 or Leu145 (Fig. 6F and G). In conclusion, Arg side chain shows a large flexibility which allows to form different electrostatic interactions. Further details are reported in Table 5.

The X-ray structure of the reduced form of *Ph*SOD (Fe(II)*Ph*SOD) has also been determined. Unsurprisingly, the two dimers in the a.u. are strictly similar to each other and to the structure of Fe(III)*Ph*SOD. The similarity includes the position of active site residues and of many solvent molecules. A detailed comparison of the geometry of the iron coordination sphere, including values observed in the reduced and oxidized forms of *Ec*SOD, is reported in Table 6. In this comparison we have supposed that photoreduction of the oxidized form of *Ph*SOD is negligible, based on the following literature data: i) XANES data collected on

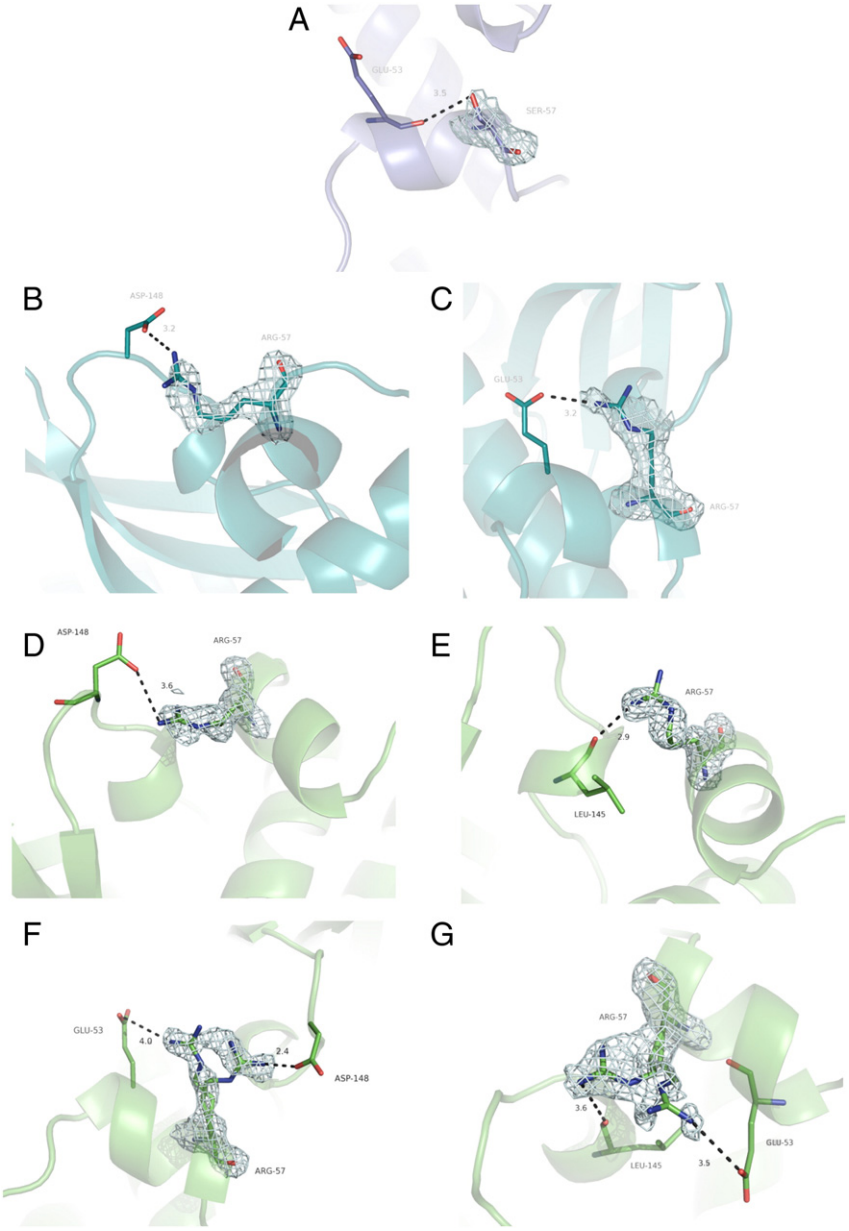

Fig. 6. Omit Fo–Fc electron density maps of the mutation site of *Ph*SOD mutants contoured at 4.0 σ level. (A) Ser57 in C57S. (B) and (C) Arg57 in C57R-form-II, chain A and B respectively. (D), (E), (F) and (G) Arg57 in C57R-form-I, chain A, B, C and D, respectively.

FeSOD from *E. coli* have revealed that ferric center undergoes a slow photoreduction at pH 7, with a rate of photoreduction equal to 3% per hour, with less than 20% of the ferric iron being reduced during the course of data collection and ii) no detectable photoreduction occurred for samples at basic pHs [26].

Our data indicate that the bond lengths and angles do not change significantly between Fe(III) and Fe(II)SODs, although a slight increase of the average Fe–ligand distances is observed in the reduced form of the enzyme. This is consistent with previous observations by Lah and coworkers [17]. Redox-coupled conformational effects are suggested to be fairly small also by other authors that have compared the oxidized and reduced form of FeSOD from *E. coli* using NMR data [27].

4. Discussion

Psychrophilic organisms produce cold-adapted enzymes that display a high catalytic efficiency at low temperature [28]. These enzymes are particularly useful to investigate the relationships between stability, dynamics and function [5].

In a previous paper [8], we have compared the structure and stability of the cold adapted iron superoxide dismutase from *P. haloplanktis* with those of the corresponding enzymes from *E. coli* [17] and from the psychrophilic organism *Aliivibrio salmonicida* [29]. We have demonstrated that *Ph*SOD has an unusual thermal stability [8]. The comparative analysis of the structure of *Ph*SOD with that of the cold adapted SOD from *A. salmonicida* [29] has suggested that the origin of the unusual stability of the former enzyme could be the presence of a number of charged residues on the protein surface [8].

Here a structural and stability study of two *Ph*SOD mutants, where Cys57 was replaced by serine or arginine, has been reported. The Cys→Arg substitution converts this amino acid position as that present in *Ec*SOD and adds a positive charge in a region of the protein that is rich in negative charged residues (Cys57 is close to Glu53 and Asp148) (Fig. 1). The Cys→Ser substitution was investigated as a control, being Cys and Ser isosteric residues. As expected, this substitution has no

Table 5
Details of the interactions of Arg57 in C57R-I.

C57R-I			
Arg A57	NH1	Asp A148 (OD1)	–
	NH2	Water	Val A150 (O)
			Asp A147 (O)
Arg B57	NH1	Leu B145 (O)	–
		Water	Asp B148 (OD1)
	NH2	Water	–
Arg C57 *Conformation A*	NH2	Asp C148 (OD1)	–
		Water	Gly C149 (N)
	NE	Water	Thr C146 (O)
Arg C57 *Conformation B*	NH1	Glu C53 (OE1)	–
		Water	Glu C53 (OE1)
	NH2	Water	–
Arg D57 *Conformation A*	NH1	Asp D148 (OD1)	–
	NE	Leu D145 (O)	–
	NH2	Water	Gly D149 (N)
		Water	Leu D145 (O)
Arg D57 *Conformation B*	NH1	Glu d53 (OE1)	–

significant effect on the structure and stability of the protein. On the other hand, the C57R mutation has significant effects on thermal stability and resistance to denaturants of the enzyme.

Presence of cysteine residues in SODs has drawn considerable attention. In many Cu/Zn SODs the removal of a free cysteine enhances protein stability and increases protein resistance toward irreversible thermal inactivation [14,30], an effect likely correlated to the low probability of non-native disulfide bonds formation. To date, no structural data on the substitution of a free cysteine residue in Fe/Mn SODs have been reported. In the present study C57R shows a higher T_{m1} and a lower T_{m2} when compared to *Ph*SOD and C57S. Furthermore, it has a higher stability against GdnHCl-induced unfolding and a lower resistance to urea-induced unfolding. These properties are coupled to a slightly lower SOD activity [12].

Pedersen et al. have ascribed the presence of two thermal transitions in the denaturation curve of *Ec*SOD to a potential reduction of iron atoms during the data collection [29]. In line with this hypothesis, denaturation curves of Fe-substituted MnSODs present two T_m (63 °C and 87 °C) that are attributed to a minor Fe(II) species and a major Fe(III) species, respectively [31]. In order to evaluate this hypothesis, we recorded the denaturation curves of *Ph*SOD in the presence of dithionite and no variations of the protein spectral features are observed. This agrees well with the finding that the X-ray structure of the reduced form of *Ph*SOD is basically identical to that of the oxidized form, with only small changes in the values of iron–ligand distances. These results are consistent with those obtained comparing oxidized and reduced structures of other SODs [17,32], and with a number of experimental data collected on Fe-substituted MnSOD (e.g. [33,34]), which altogether reveal that structural differences between reduced and oxidized Fe substituted forms are not significant. Thus the data suggest that the hypothesis proposed by Pedersen et al. [29] should be revisited. As reported in a previous paper [35], we suggest that the thermal denaturation curves of *Ec*SOD and *Ph*SOD could be interpreted using a three-state unfolding model $D \rightarrow D^* \rightarrow A$, in which D is the native dimer, D^* is a partially unfolded dimer, i.e. a dimer with a different three-dimensional arrangement with respect to the folded protein, and A is an aggregated unfolded state.

This is in line with models reported in the literature, which propose that the destabilization of other SODs results in aggregation and disease [30].

Several characteristics of the melting behavior of *Ph*SOD and its mutants are consistent with this scheme: (1) the sample does not refold upon complete or partial unfolding ([8] and present work); (2) the loss of enzymatic activity and the first transition are roughly synchronous ([8] and present work); (3) the second transition depends on protein concentration, thus suggesting the presence of an aggregation process, and indeed aggregates are visible in the sample cells after heating at high temperatures ([8] and present work); (4) at the temperature corresponding to the first transition *Ph*SOD retains a dimeric state ([8] and present work); (5) the existence of intermediates whose mass is comparable to that of the native enzyme has been already observed in the unfolding pathway of other SODs [35]; and (6) the chromatographic behavior of other SODs depends on the enzyme concentration, thus suggesting the existence of a more complex structural organization of this enzyme [36,37]. According to the three-state model that we propose, the experimental data collected for C57R show an increased stability of the native dimeric state and a significantly lower thermal tolerance of the partially unfolded dimer formed upon the first transition. Since C57R is slightly less active than *Ph*SOD [12] and taking into account that a correctly folded dimer is essential for the catalytic activity of iron SODs, these findings are in agreement with the frequently observed inverse relation between stability and activity of enzymes (e.g. [38]). Furthermore, as most psychrophilic enzymes optimize their activity at low temperatures by increasing the active site flexibility or by destabilizing the whole molecule [28], the reduced catalytic activity of C57R could be also related to the increased thermal stability of the dimer.

The crystals of C57R were grown in the presence of ammonium sulfate, condition in which a significant screening of electrostatic interactions is expected, and in a different ionic strength condition, containing PEG as a precipitant. Salt-bridges are present in both cases, although the Arg side chain is found to adopt alternative conformations. These data give a dynamic scenario of salt bridges on the protein surface, where charged residues can move apart and then get closer thus forming a network that contributes to stabilize C57R. It is well known that the presence of favorable interactions among charged groups placed on the protein surface is the specific tool to cope with high temperature [39–41]. In this respect, it should be also recalled that

Table 6
Metal coordination geometry. Average distance values in Å are calculated on independent chains in the asymmetric unit. Standard deviations are reported in parentheses.

	*Ph*SOD-I (3LIO)	*Ph*SOD-II (3LJF)	C57S (4L2B)	C57R-I (4L2C)	C57R-II (4L2A)	Fe(II)*Ph*SOD (4L2D)	Fe(III)*Ec*SOD (1ISB)	Fe(II)*Ec*SOD (1ISA)
Fe–$N^{\varepsilon 2}$ (His 26)	2.11 (0.08)	2.13 (0.06)	2.11 (0.01)	2.09 (0.05)	2.10 (0.01)	2.14 (0.06)	2.16 (0.01)	2.18 (0.01)
Fe–$N^{\varepsilon 2}$ (His 73)	2.07 (0.08)	2.07 (0.05)	2.09 (0.01)	2.07 (0.01)	2.07 (0.01)	2.14 (0.04)	2.04 (0.02)	2.04 (0.02)
Fe–$O^{\delta 2}$ (Asp 157)	1.94 (0.1)	1.95 (0.06)	1.72 (0.01)	1.98 (0.04)	1.71 (0.02)	1.99 (0.09)	1.91 (0.03)	1.93 (0.02)
Fe–$N^{\varepsilon 2}$ (His 161)	2.12 (0.13)	2.10 (0.09)	2.11 (0.01)	2.16 (0.10)	2.10 (0.01)	2.16 (0.05)	2.07 (0.01)	2.12 (0.01)
Fe–OH_2	2.14 (0.08)	2.21 (0.13)	2.29 (0.11)	2.15 (0.09)	2.25 (0.10)	2.27 (0.08)	1.95 (0.05)	2.04 (0.02)

electrostatic interactions have been considered to play a major role in the thermostability of Cu,Zn SOD from *Alvinella pompejana* [42]. Accordingly, optimization of surface charges could be the factor affecting the stability of the first transition of C57R. On the other hand, when the protein partially denatures the charged Arg residues are free to interact with residues of other protein molecules, favoring the formation of intermolecular aspecific contacts that are likely responsible for protein aggregation. The presence of additional salt bridges on the protein surface of C57R can be also used to rationalize the higher stability of C57R against GdnHCl-induced unfolding. In fact, it has been proposed that this denaturant functions by interacting with surface charged residues [43,44]. The stabilizing role of the charge–charge networks in C57R agrees with its slightly lower resistance to the action of a neutral denaturant, such as urea, when compared to *Ph*SOD. In this respect, it should be also noted that the ratio between $C_{1/2}$ values obtained using urea and GdnHCl is significantly smaller in C57R ($[urea]_{1/2}/[GdnHCl]_{1/2}$ is 1.5–1.6) with respect to *Ph*SOD ($[urea]_{1/2}/[GdnHCl]_{1/2}$ is about 2.3) and to that (approximately equal to 2) obtained from analyses carried out on several different proteins [45].

It is interesting to note that in the case of *Ec*SOD the side chain of Arg57 is not involved in any salt bridge. The absence of the interaction with Asp148 observed in C57R is related to the different conformation of the 144–152 loop, which is in turn caused by the insertion of Gly149.

5. Conclusions

The simultaneous use of spectroscopic methods and X-ray crystallography has clarified the effect of Cys57 mutation on the structure and stability of *Ph*SOD. In particular, by substituting Cys57 with Arg, salt bridges can be formed on the protein surface. These interactions cause an increase in the temperature of the first transition midpoint and an enhanced stability against GdnHCl of the mutant. The results confirm the hypothesis that optimization of surface charges could be the key factor for the high thermal stability of *Ph*SOD. It is also interesting to stress that the ionic strength of crystallization medium does not influence the ion pairing phenomenon on the protein surface.

Finally, our data show that no significant structural and spectral differences occur between oxidized and reduced forms of the enzyme, an issue suggesting that the three-state unfolding of SODs cannot be ascribed to a different reduction state of the coordinated metal ion.

Acknowledgements

We express our gratitude to Francesca Coscia, Valentina Doria and Elisa Giugliano for their help in the early stages of the fluorescence measurements. Giosuè Sorrentino and Maurizio Amendola (Institute of Biostructures and Bioimaging, Naples, Italy) and the staff of the Elettra beam-line XRD1 are also gratefully acknowledged for technical assistance.

References

[1] S. D'Amico, T. Collins, J.C. Marx, G. Feller, C. Gerday, Psychrophilic microorganisms: challenges for life, EMBO Rep. 7 (2006) 385–389.
[2] G. Feller, Life at low temperatures: is disorder the driving force? Extremophiles 11 (2007) 211–216.
[3] J.C. Marx, V. Blaise, T. Collins, S. D'Amico, D. Delille, E. Gratia, A. Hoyoux, A.L. Huston, G. Sonan, G. Feller, C. Gerday, A perspective on cold enzymes: current knowledge and frequently asked questions, Cell. Mol. Biol. (Noisy-le-grand) 50 (2004) 643–655.
[4] A.L. Huston, J.Z. Haeggstrom, G. Feller, Cold adaptation of enzymes: structural, kinetic and microcalorimetric characterizations of an aminopeptidase from the Arctic psychrophile *Colwellia psychrerythraea* and of human leukotriene A(4) hydrolase, Biochim. Biophys. Acta 1784 (2008) 1865–1872.
[5] K.S. Siddiqui, R. Cavicchioli, Cold-adapted enzymes, Annu. Rev. Biochem. 75 (2006) 403–433.
[6] R. Cavicchioli, Cold-adapted archaea, Nat. Rev. Microbiol. 4 (2006) 331–343.
[7] E. De Vendittis, I. Castellano, R. Cotugno, M.R. Ruocco, G. Raimo, M. Masullo, Adaptation of model proteins from cold to hot environments involves continuous and small adjustments of average parameters related to amino acid composition, J. Theor. Biol. 250 (2008) 156–171.
[8] A. Merlino, I. Russo Krauss, I. Castellano, E. De Vendittis, B. Rossi, M. Conte, A. Vergara, F. Sica, Structure and flexibility in cold-adapted iron superoxide dismutases: the case of the enzyme isolated from *Pseudoalteromonas haloplanktis*, J. Struct. Biol. 172 (2010) 343–352.
[9] I. Castellano, A. Di Maro, M.R. Ruocco, A. Chambery, A. Parente, M.T. Di Martino, G. Parlato, M. Masullo, E. De Vendittis, Psychrophilic superoxide dismutase from *Pseudoalteromonas haloplanktis*: biochemical characterization and identification of a highly reactive cysteine residue, Biochimie 88 (2006) 1377–1389.
[10] A.F. Miller, Superoxide dismutases: ancient enzymes and new insights, FEBS Lett. 586 (2012) 585–595.
[11] J.J. Perry, D.S. Shin, E.D. Getzoff, J.A. Tainer, The structural biochemistry of the superoxide dismutases, Biochim. Biophys. Acta 1804 (2010) 245–262.
[12] I. Castellano, M.R. Ruocco, F. Cecere, A. Di Maro, A. Chambery, A. Michniewicz, G. Parlato, M. Masullo, E. De Vendittis, Glutathionylation of the iron superoxide dismutase from the psychrophilic eubacterium *Pseudoalteromonas haloplanktis*, Biochim. Biophys. Acta 1784 (2008) 816–826.
[13] H.E. Parge, E.D. Getzoff, C.S. Scandella, R.A. Hallewell, J.A. Tainer, Crystallographic characterization of recombinant human CuZn superoxide dismutase, J. Biol. Chem. 261 (1986) 16215–16218.
[14] D.E. McRee, S.M. Redford, E.D. Getzoff, J.R. Lepock, R.A. Hallewell, J.A. Tainer, Changes in crystallographic structure and thermostability of a Cu,Zn superoxide dismutase mutant resulting from the removal of a buried cysteine, J. Biol. Chem. 265 (1990) 14234–14241.
[15] I. Russo Krauss, A. Merlino, A. Vergara, F. Sica, An overview of biological macromolecule crystallization, Int. J. Mol. Sci. 14 (2013) 11643–11691.
[16] A. Merlino, I. Russo Krauss, I. Castellano, E. De Vendittis, A. Vergara, F. Sica, Crystallization and preliminary X-ray diffraction studies of a psychrophilic iron superoxide dismutase from *Pseudoalteromonas haloplanktis*, Protein Pept. Lett. 15 (2008) 415–418.
[17] M.S. Lah, M.M. Dixon, K.A. Pattridge, W.C. Stallings, J.A. Fee, M.L. Ludwig, Structure–function in *Escherichia coli* iron superoxide dismutase: comparisons with the manganese enzyme from *Thermus thermophilus*, Biochemistry 34 (1995) 1646–1660.
[18] Z. Otwinowsky, W. Minor, Processing of X-ray diffraction data collected in oscillation mode, Methods Enzymol. (1997) 307–326.
[19] A.T. Brunger, P.D. Adams, G.M. Clore, W.L. DeLano, P. Gros, R.W. Grosse-Kunstleve, J.S. Jiang, J. Kuszewski, M. Nilges, N.S. Pannu, R.J. Read, L.M. Rice, T. Simonson, G.L. Warren, Crystallography & NMR system: a new software suite for macromolecular structure determination, Acta Crystallogr. D Biol. Crystallogr. 54 (Pt 5) (1998) 905–921.
[20] G.N. Murshudov, A.A. Vagin, E.J. Dodson, Refinement of macromolecular structures by the maximum-likelihood method, Acta Crystallogr. D Biol. Crystallogr. 53 (Pt 3) (1997) 240–255.
[21] T.A. Jones, M. Bergdoll, M. Kjeldgaard, O: a macromolecule modeling environment, in: C. Bugg, S. Ealick (Eds.), Crystallogr Model Methods Mol Des, [Pap Symp], Springer-Verlag Press, 1990, pp. 189–199.
[22] P. Emsley, B. Lohkamp, W.G. Scott, K. Cowtan, Features and development of Coot, Acta Crystallogr. D Biol. Crystallogr. 66 (Pt 4) (2010) 486–501.
[23] R.A. Laskowski, M.W. MacArthur, M.D. Moss, J.M. Thorton, PROCHECK: a program to check the stereochemical quality of protein structure, J. Appl. Crystallogr. 26 (1993) 283–291.
[24] J.M. McCord, I. Fridovich, Superoxide dismutase. An enzymic function for erythrocuprein (hemocuprein), J. Biol. Chem. 244 (1969) 6049–6055.
[25] A. Dello Russo, R. Rullo, G. Nitti, M. Masullo, V. Bocchini, Iron superoxide dismutase from the archaeon *Sulfolobus solfataricus*: average hydrophobicity and amino acid weight are involved in the adaptation of proteins to extreme environments, Biochim. Biophys. Acta 1343 (1997) 23–30.
[26] D.L. Tierney, J.A. Fee, M.L. Ludwig, J.E. Penner-Hahn, X-ray absorption spectroscopy of the iron site in *Escherichia coli* Fe(III) superoxide dismutase, Biochemistry 34 (1995) 1661–1668.
[27] S. Vathyam, R.A. Byrd, A.F. Miller, Mapping the effects of metal ion reduction and substrate analog binding to Fe-superoxide dismutase by NMR spectroscopy, Magn. Reson. Chem. 38 (2000) 536–542.
[28] C. Struvay, G. Feller, Optimization to low temperature activity in psychrophilic enzymes, Int. J. Mol. Sci. 13 (2012) 11643–11665.
[29] H.L. Pedersen, N.P. Willassen, I. Leiros, The first structure of a cold-adapted superoxide dismutase (SOD): biochemical and structural characterization of iron SOD from *Aliivibrio salmonicida*, Acta Crystallogr. Sect. F: Struct. Biol. Cryst. Commun. 65 (2009) 84–92.
[30] M. DiDonato, L. Craig, M.E. Huff, M.M. Thayer, R.M. Cardoso, C.J. Kassmann, T.P. Lo, C.K. Bruns, E.T. Powers, J.W. Kelly, E.D. Getzoff, J.A. Tainer, ALS mutants of human superoxide dismutase form fibrous aggregates via framework destabilization, J. Mol. Biol. 332 (2003) 601–615.
[31] K. Mizuno, M.M. Whittaker, H.P. Bachinger, J.W. Whittaker, Calorimetric studies on the tight binding metal interactions of *Escherichia coli* manganese superoxide dismutase, J. Biol. Chem. 279 (2004) 27339–27344.
[32] M.L. Ludwig, A.L. Metzger, K.A. Pattridge, W.C. Stallings, Manganese superoxide dismutase from *Thermus thermophilus*. A structural model refined at 1.8 A resolution, J. Mol. Biol. 219 (1991) 335–358.
[33] C.K. Vance, A.F. Miller, Spectroscopic comparisons of the pH dependencies of Fe-substituted (Mn)superoxide dismutase and Fe-superoxide dismutase, Biochemistry 37 (1998) 5518–5527.
[34] C.K. Vance, A.F. Miller, Novel insights into the basis for *Escherichia coli* superoxide dismutase's metal ion specificity from Mn-substituted FeSOD and its very high E(m), Biochemistry 40 (2001) 13079–13087.
[35] A. Merlino, I. Russo Krauss, B. Rossi, A. Vergara, A. De Vendittis, S. Marco, E. De Vendittis, F. Sica, Identification of an active dimeric intermediate populated during

the unfolding process of the cambialistic superoxide dismutase from *Streptococcus mutans*, Biochimie 94 (2012) 768–775.
[36] A. De Vendittis, M. Amato, A. Mickniewicz, G. Parlato, A. De Angelis, I. Castellano, R. Rullo, F. Riccitiello, S. Rengo, M. Masullo, E. De Vendittis, Regulation of the properties of superoxide dismutase from the dental pathogenic microorganism *Streptococcus mutans* by iron- and manganese-bound co-factor, Mol. Biosyst. 6 (2010) 1973–1982.
[37] A. De Vendittis, S. Marco, A. Di Maro, A. Chambery, A. Albino, M. Masullo, A. Michniewicz, G. Parlato, A. De Angelis, E. De Vendittis, R. Rullo, Properties of a putative cambialistic superoxide dismutase from the aerotolerant bacterium *Streptococcus thermophilus* strain LMG 18311, Protein Pept. Lett. 19 (2012) 333–344.
[38] P. Zavodszky, J. Kardos, Svingor, G.A. Petsko, Adjustment of conformational flexibility is a key event in the thermal adaptation of proteins, Proc. Natl. Acad. Sci. U. S. A. 95 (1998) 7406–7411.
[39] E. Bae, G.N. Phillips Jr., Structures and analysis of highly homologous psychrophilic, mesophilic, and thermophilic adenylate kinases, J. Biol. Chem. 279 (2004) 28202–28208.
[40] D. Georlette, B. Damien, V. Blaise, E. Depiereux, V.N. Uversky, C. Gerday, G. Feller, Structural and functional adaptations to extreme temperatures in psychrophilic, mesophilic, and thermophilic DNA ligases, J. Biol. Chem. 278 (2003) 37015–37023.
[41] L.D. Unsworth, J. van der Oost, S. Koutsopoulos, Hyperthermophilic enzymes—stability, activity and implementation strategies for high temperature applications, FEBS J. 274 (2007) 4044–4056.
[42] D.S. Shin, M. Didonato, D.P. Barondeau, G.L. Hura, C. Hitomi, J.A. Berglund, E.D. Getzoff, S.C. Cary, J.A. Tainer, Superoxide dismutase from the eukaryotic thermophile *Alvinella pompejana*: structures, stability, mechanism, and insights into amyotrophic lateral sclerosis, J. Mol. Biol. 385 (2009) 1534–1555.
[43] J.K. Myers, C.N. Pace, J.M. Scholtz, Denaturant m values and heat capacity changes: relation to changes in accessible surface areas of protein unfolding, Protein Sci. 4 (1995) 2138–2148.
[44] E.P. O'Brien, R.I. Dima, B. Brooks, D. Thirumalai, Interactions between hydrophobic and ionic solutes in aqueous guanidinium chloride and urea solutions: lessons for protein denaturation mechanism, J. Am. Chem. Soc. 129 (2007) 7346–7353.
[45] V. Granata, P.D. Vecchio, G. Barone, E. Shehi, P. Fusi, P. Tortora, G. Graziano, Guanidine-induced unfolding of the Sso7d protein from the hyperthermophilic archaeon *Sulfolobus solfataricus*, Int. J. Biol. Macromol. 34 (2004) 195–201.